Supporting online material for 'Air-mediates the impact of a compliant hemisphere on a rigid smooth surface'

Siqi Zheng[1], Sam Dillavou[2], John M. Kolinski[1]

February 26, 2021

1 COMPRESSED FRAME STACK (CFS) IMAGES

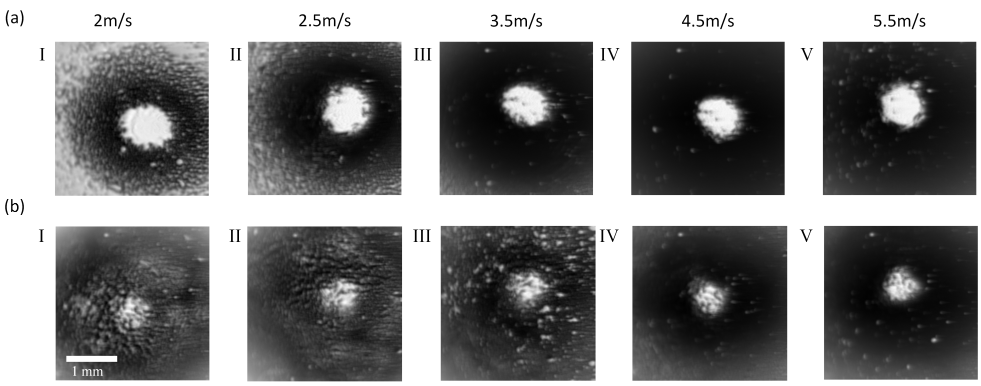

Figure S 1. Compressed Frame Stack (CFS) images of elastic impactor with different elasticity at different impact velocities.(a)'Elite Double 8'($E = 250$ kPa, 'soft,' $c_R = 7.9$ m/s) (b)'Elite Double 32' ($E = 1.1$MPa, 'hard,' $c_R = 16.6$ m/s)

2 MEASUREMENT OF r_0 USING RAYS EMANATING FROM IMPACT CENTER

At the onset of impact, the initial contact forms a patchy ring. To accurately measure the initial radius of the contact ring, a precise measurement of the impact center is essential. The initial radius r_0 is determined from the intensity minimum of the CFS along rays emanating from the impact center. The median value over all angles defines r_0, as shown in Fig. S2.

[1] *The Institute of Mechanical Engineering, École Polytechnique Fédérale de Lausanne, 1015 Lausanne, Switzerland*
[2] *Department of Physics, Harvard University, Cambridge, Massachusetts 02138, USA*

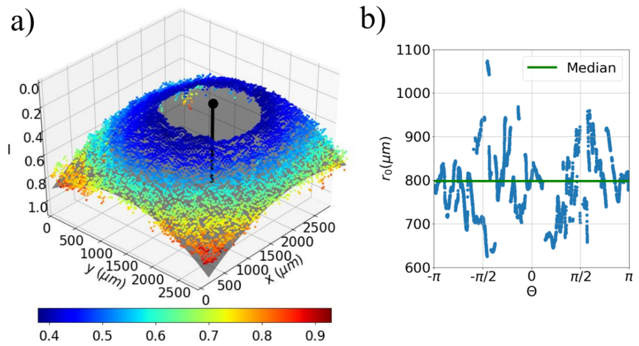

Figure S 2. Determining r_0 from the compressed frame stack (CFS). (a) The intensity map of the CFS shown in Fig 1 (b) is plotted in color and 3D. A paraboloid fit to the data is shown in gray; the axis of the paraboloid defines the impact axis of symmetry, indicated by the black point at the center of the contact ring. (b) Radial location of the intensity minimum along traces emanating from the center of the contact ring to each pixel on the edge of the CFS are shown unwrapped as a function of Θ, the distance of the lowest-intensity pixel from the center is defined as the initial contact ring radius r_0 for each intensity trace. The initial contact ring radius of all minima thus obtained are plotted; r_0 is defined from the median of these values.

3 TRAILING CONTACT FRONTS

The contact front trails behind the deformation front; the difference between the two fronts depends on the elastic modulus at a given V. The overhang front appears to follow the $\sim \sqrt{t}$ dictated by the impactor's hemispherical geometry, as shown in Fig. S4 (b). The contact front trails behind this, as can be seen from the measured front in Fig. S3 (c). For impacts with the hard and soft impactor at 2 m/sec, we show the deformation front (identical for both), the measured data (points) and local low-order polynomial fits (dashed lines), as shown in Fig. S4 (d).

The contact fronts then grow outward beneath this overhang, and typically catch up with the deformation front at later times. We monitor the difference between these fronts to quantify the error from the VFT, as shown in Fig. S4 (a).

The position of the deformation front at the leading edge of the overhang, and the contact fronts, is determined from the space-time graphs in Fig. S3 (a) II. The deformation front advances with the scaling determined by the impactor's geometry at $r \propto \sqrt{t}$; this is shown with the advancing contact fronts for the hard and soft impactors in Fig. S4 (b).

At sufficiently high V, the contact front undergoes a transition from super-Rayleigh to sub-Rayleigh advancing velocities. This can be clearly seen in the compressed frame stacks (CFS) plotted in Fig. 4 of the main text. Here, we show several random traces from the CFS in intensity-r coordinates. The pronounced increase in the range of contact front transition times is clearly captured beyond $r = r^*$, as can be seen in Fig. S5.

4 PROFILOMETRY AND QUASI-STATIC VFT IMAGE

The textures observed during impact raise an important question: are these textures a consequence of the dynamical interaction between the elastomer and the air film, or are they intrinsic to the impactor's surface?

We carry out two key experiments to probe this possibility, and test whether these textures are a dynamic phenomenon, or a consequence of intrinsic textures on the impactor's surface. First, we use white-light interferometric profilometry (Nikon Ti-Eclipse with 10X Nikon CF IC Epi Plan DI Interferometry Objective) to observe the impactor's surface at the smallest scales. We show an area of 1.8 mm x 1.8 mm at the tip of the impactor. Color corresponds to the height of the surface from a reference plane, measured in nm, as can be seen in Fig. S6

A second test can further evaluate the role of the impator's intrinsic texture. Here, we drive the impactor toward the surface quasi-statically (effectively at a velocity of 1 mm/sec), and generate a compressed frame stack with an exposure time of 2 seconds shown in Fig. S7 b)side-by-side with a 1.5 m/sec impact of the soft elastomer shown in Fig. S7 a). While the texture observed in the dynamic impact is clearly absent, this can be quantiatively shown by taking an intensity trace from the impact centers of these two CFSs, as shown in Fig. S7 c). Here we see that the quasistatic impact front is stable and low-noise, whereas the dynamic impact event is strongly punctuated by dynamic rupture of the air film due to an elasto-lubricative instability.

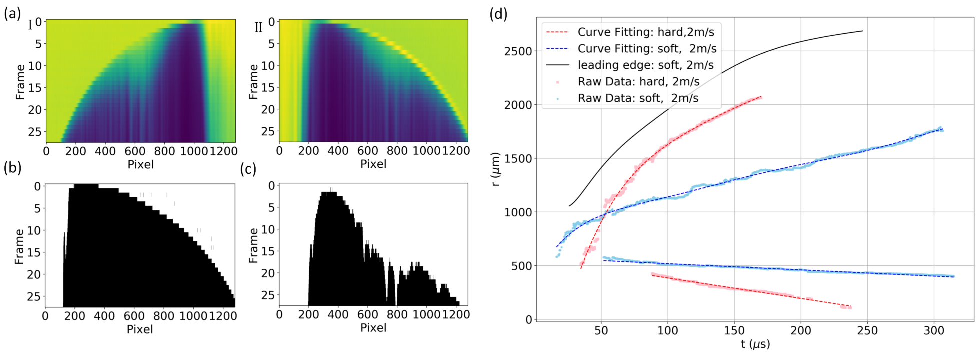

Figure S 3. Deformation front and contact fronts for two 2 m/sec impact events. a) An instantaneous snapshot recorded with a high-speed camera that enables direct visualization of the overhang feature (grayscale, as indicated). The approximate impact center is indicated with a red circle; the overhang front appears only on the left-hand side of the image, as indicated by the green dashed line. The ellipses indicate that only a narrow strip of the impact event is captured, reflecting the trade-off between frame rate and field-of-view for traditional high-speed imaging. b) Space-time plots of the intensity along r for two $V = 2$ m/sec impacts of the soft impactor (I & II). The leading edge of the overhang exceeds the advancing contact front at early times, visible by the greyscale intensity (green color), intermediate between far (yellow) and contact (dark blue). The inward moving fronts progress at approximately 0.1 c_R. Notably, the leading edge of the overhang appears to follow the anticipated $\sqrt{t}$ dictated by the impactor's geometry. c) The deformation front at the leading edge of the overhang region is extracted from high-speed imaging data similar such as those shown in (a). d) The contact front corresponding to the overhang in (a) is plotted as a function of time. e) The deformation front (black line) is shown well-ahead of the contact fronts for the soft (blue) and hard (red) impactors; measurements are indicated with points, while low-order polynomial fits are shown in dashed lines.

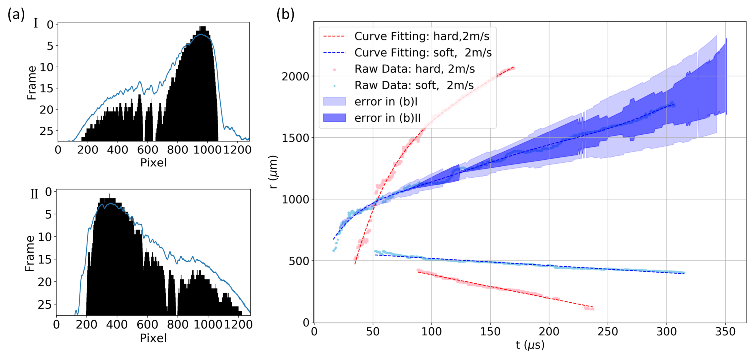

Figure S 4. Overhang fronts vs. contact fronts for two $V = 2$ m/sec impacts of the soft impactor (I & II). a) The contact fronts are extracted using an aggressive threshold near the lowest intensity value in the space-time graph shown in Fig. S3 a). The equivalent 1-D CFS is shown in the blue lines, showing the emergent discrepancy between the VFT recovered front position and the instantaneous front position. This discrepancy arises from the intermediate intensity values recorded from the TIR imaging modality when the impactor enters the evanescent field. We use this discrepancy to construct an error estimate for the front position. b) The contact front position (blue points), along with the error estimates (blue rectangles) for events (I & II) are plotted vs. t.

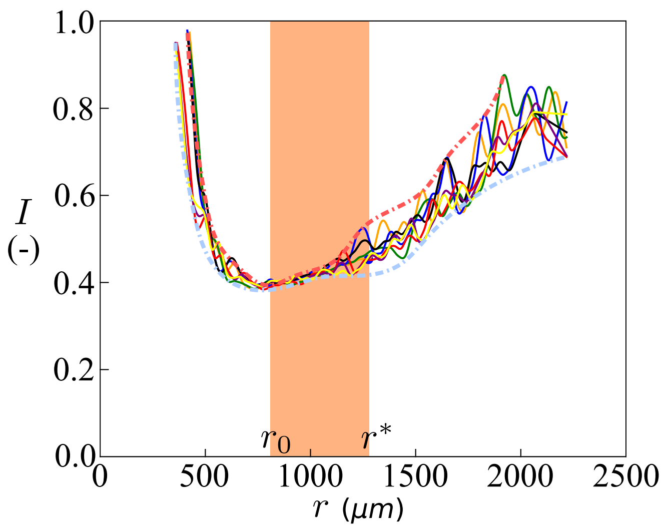

Figure S 5. Several $I - r$ traces for a high-velocity impact with the soft impactor at $V = 2.5$ m/sec. The original contact radius r_0, as well as the radius r^* when the contact front decelerates below c_R are indicated by the boundaries of the orange region. Clearly, the transition time when contact occurs has enhanced variability when $r > r^*$, as can be seen by the bounding lines of these traces in the dashed blue and red curves that serve as guides to the eye.

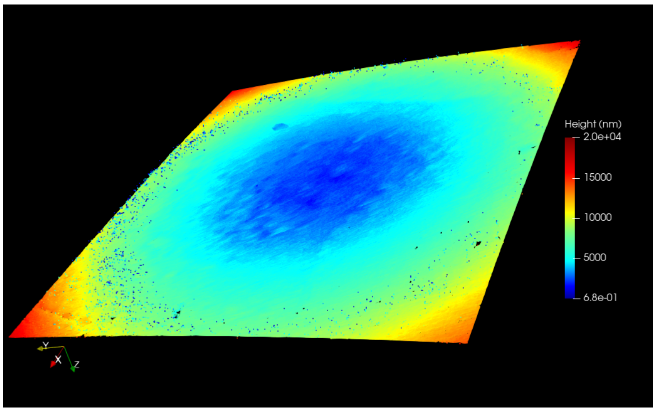

Figure S 6. A 1.8 mm x 1.8 mm area of the impactor's surface is shown in oblique view, as measured with white-light interferometric profilometry. The surface contours show some texture, but this texture does not correspond to the lateral scales observed in the experiments shown in e.g. Fig. S2. The axes are shown to scale.

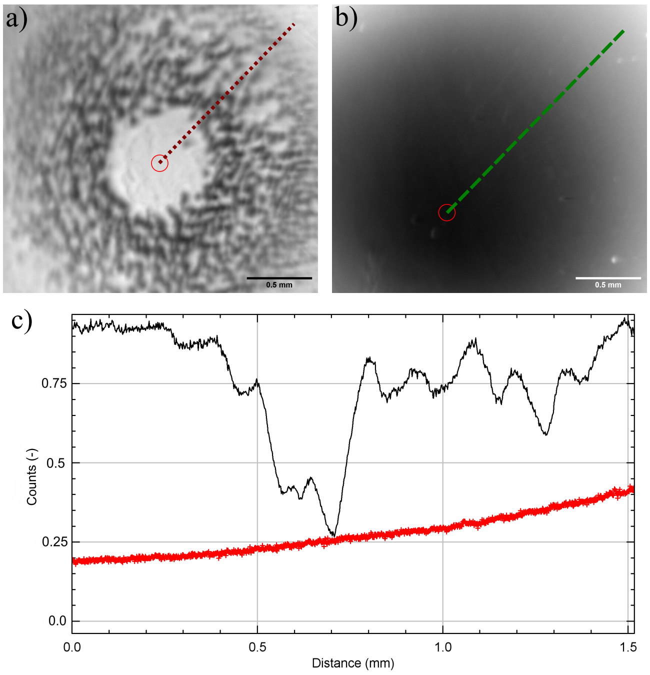

Figure S 7. Comparison of dynamic and quasi-static impact events. a) Here, the CFS for a quasi-static impact event is shown, with pronounced texture that emerges during the impact dynamics. b) Such dynamic textures are absent for the quasi-static experiment, where the impactor is driven toward the surface at a constant and very low (1 mm/sec) velocity. c) Intensity traces show the pronounced difference between the dynamically emerging texture (black) and the very smooth progress of the contact front (red) for the dynamic and quasi-static experiments, respectively.